Steel and Composite Structures, *Vol. 20, No. 3 (2016) 623-649*
DOI: http://dx.doi.org/10.12989/scs.2016.20.3.623

Using an equivalent continuum model for 3D dynamic analysis of nanocomposite plates

Vahid Tahouneh*

Young Researchers and Elite Club, *Islamshahr Branch*, *Islamic Azad University*, *Islamshahr*, *Iran*

(*Received February 26, 2014, Revised November 12, 2015, Accepted November 27, 2015*)

Abstract. Most of the early studies on plates vibration are focused on two-dimensional theories, these theories reduce the dimensions of problems from three to two by introducing some assumptions in mathematical modeling leading to simpler expressions and derivation of solutions. However, these simplifications inherently bring errors and therefore may lead to unreliable results for relatively thick plates. The main objective of this research paper is to present 3-D elasticity solution for free vibration analysis of continuously graded carbon nanotube-reinforced (CGCNTR) rectangular plates resting on two-parameter elastic foundations. The volume fractions of oriented, straight single-walled carbon nanotubes (SWCNTs) are assumed to be graded in the thickness direction. In this study, an equivalent continuum model based on the Eshelby-Mori-Tanaka approach is employed to estimate the effective constitutive law of the elastic isotropic medium (matrix) with oriented, straight carbon nanotubes (CNTs). The proposed rectangular plates have two opposite edges simply supported, while all possible combinations of free, simply supported and clamped boundary conditions are applied to the other two edges. The formulations are based on the three-dimensional elasticity theory. A semi-analytical approach composed of differential quadrature method (DQM) and series solution is adopted to solve the equations of motion. The fast rate of convergence of the method is demonstrated and comparison studies are carried out to establish its very high accuracy and versatility. The 2-D differential quadrature method as an efficient and accurate numerical tool is used to discretize the governing equations and to implement the boundary conditions. The convergence of the method is demonstrated and to validate the results, comparisons are made between the present results and results reported by well-known references for special cases treated before, have confirmed accuracy and efficiency of the present approach. The novelty of the present work is to exploit Eshelby-Mori-Tanaka approach in order to reveal the impacts of the volume fractions of oriented CNTs, different CNTs distributions, various coefficients of foundation and different combinations of free, simply supported and clamped boundary conditions on the vibrational characteristics of CGCNTR rectangular plates. The new results can be used as benchmark solutions for future researches.

Keywords: analytical methods; Mori-Tanaka scheme; three-dimensional free vibration; continuously graded carbon nanotube-reinforced (CGCNTR); two-parameter elastic foundation

1. Introduction

Recently, Nanocomposites have significant importance for engineering applications that require high levels of structural performance and multi-functionality. Carbon nanotubes (CNTs) have demonstrated exceptional mechanical, thermal and electrical properties. These materials are

*Corresponding author, Ph.D. Student, E-mail: vahid.th1982@gmail.com; vahid.tahouneh@ut.ac.ir

Copyright © 2016 Techno-Press, Ltd.
http://www.techno-press.org/?journal=scs&subpage=6 ISSN: 1229-9367 (Print), 1598-6233 (Online)

considered as one of the most promising reinforcement materials for high performance structural and multifunctional composites with vast application potentials (Esawi and Farag 2007). A detailed summary of the mechanical properties of CNTs can be found in (Salvetat and Rubio 2002). The exceptional mechanical properties of CNTs have shown great promise for a wide variety of applications, such as nanotransistors, nanofillers, semiconductors, hydrogen storage devices, structural materials, molecular sensors, field-emission-based displays, and fuel cells, to name just a few (Endo *et al*. 2004). The addition of nano-sized fibers or nanofillers, such as CNTs, can further increase the merits of polymer composites (Wernik and Meguid 2011). These nanocomposites, easily processed due to the small diameter of the CNTs, exhibit unique properties (Thostenson *et al*. 2001, Moniruzzaman and Winey 2006), such as enhanced modulus and tensile strength, high thermal stability and good environmental resistance. This behavior, combined with their low density makes them suitable for a broad range of technological sectors such as telecommunications, electronics (Valter *et al*. 2002) and transport industries, especially for aeronautic and aerospace applications where the reduction of weight is crucial in order to reduce the fuel consumption. For example, Qian *et al*. (2000) showed that the addition of 1wt.% (i.e., 1% by weight) multiwall CNT to polystyrene resulted in 36-42% and ~25% increases in the elastic modulus and the break stress of the nanocomposite properties, respectively. In addition, Yokozeki *et al*. (2007) reported the retardation of the onset of matrix cracking in the composite laminates containing the cup-stacked CNTs compared to those without the cup-stacked CNTs. Most studies on CNT-reinforced composites (CNTRCs) have focused on their material properties (Hu *et al*. 2005, Fidelus *et al*. 2005, Bonnet *et al*. 2007, Han and Elliott 2007, Odegard *et al*. 2003). Jin and Yuan (2003) determined the elasticity properties of single wall CNTs applying the molecular dynamic method. In fact, this macroscopic behavior was analyzed by studying the interaction of the atomic force and dynamic response in nanostructures affected by insignificant strain. Chang and Gao (2003) studied the dependence of single wall CNT elastic properties on its dimensions according to the molecular mechanics model. In fact, this model is one of the first studies for developing the analytical method application of molecular mechanic for modeling of nanostructures. Griebel and Hamaekers (2004) analyzed the elastic modulus of composite structures under CNTs reinforcement by simulating the molecular dynamic. The research was carried out on the composite structures made of polyethylene reinforced by carbon nonotubes.

Functionally graded materials (FGMs) are a new class of advanced composite materials in which the microstructural details are spatially varied through smooth and continuous distribution of the reinforcement phase. The concept of FGM can be utilized for the management of a material's microstructure so that the vibrational behavior of a plate/shell structure made of such material can be improved. In recent years, two kinds of FGMs are designed to improve mechanical behavior of plate/shell structures. One is functionally graded fiber-reinforced composites that have a smooth variation of material volume fractions, and/or in-plane fiber orientations, through the radial direction (Sobhani Aragh *et al*. 2011, Yas and Sobhani Aragh 2010, Batra and Jin 2005, Yas and Sobhani Aragh 2010, Vel 2010). Another one is functionally graded metal/ceramic composites with continuous composition gradation from pure ceramic on one surface to full metal on the other one (Reddy and Cheng 2001, Matsunaga 2008, Jabbari *et al*. 2006). According to a comprehensive survey of literature, the authors found that there are few research studies on the mechanical behavior of functionally graded CNTRC structures. Shen (2009) for the first time suggested that the nonlinear bending behavior can be considerably improved through the use of a functionally graded distribution of CNTs in the matrix. He introduced the CNT efficiency parameter to account load transfer between the nanotube and polymeric phases. Compressive postbuckling and thermal

buckling behavior of functionally graded nanocomposite plates reinforced by aligned, straight single-walled CNTs (SWCNTs) subjected to in-plane temperature variation were reported by Shen and Zhu (2010) and Shen and Zhang (2010). They found that in some cases the CNTRC plate with intermediate CNT volume fraction does not have intermediate buckling temperature and initial thermal postbuckling strength. Moreover, Ke *et al*. (2010) investigated the nonlinear free vibration of functionally graded CNTRC Timoshenko beams. They found that both linear and nonlinear frequencies of functionally graded CNTRC beam with symmetrical distribution of CNTs are higher than those of beams with uniform or unsymmetrical distribution of CNTs. To the best of authors' knowledge the review of open literature showed that the studies on functionally graded CNTRCs were restricted to nanocomposite structures having graded aligned, straight CNTs in the thickness direction, and effective material properties of CNTRCs were estimated through the extended rule of mixture. This motivates us to employ the Eshelby-Mori-Tanaka approach to calculate the elastic stiffness properties of nanocomposite materials reinforced by graded oriented, straight CNTs.

Plates resting on elastic foundations have found considerable applications in structural engineering problems. Reinforced-concrete pavements of highways, airport runways, foundation of storage tanks, swimming pools, and deep walls together with foundation slabs of buildings are well-known direct applications of these kinds of plates. The underlying layers are modeled by a Winkler-type elastic foundation. The most serious deficiency of the Winkler foundation model is to have no interaction between the springs. In other words, the springs in this model are assumed to be independent and unconnected. The Winkler foundation model is fairly improved by adopting the Pasternak foundation model, a two-parameter model, in which the shear stiffness of the foundation is considered. A closed-form solution for the vibration frequencies of simply supported Mindlin plates on Pasternak foundations and subjected to biaxial initial stresses was presented by Xiang *et al*. (1996). The buckling load of Mindlin plates on Pasternak foundations was obtained in terms of the thin plate solution. Based on first-order shear deformation plate theory, the buckling and vibration analysis of moderately thick laminates on Pasternak foundations were presented by Xiang *et al*. (1994). The effects of foundation parameters, transverse shear deformation, and rotary inertia and the number of layers on the buckling and vibration of cross-ply laminates were examined. Wang *et al*. (1997) presented relationships between the buckling loads of simply supported plates on a Pasternak foundation determined by classical Kirchhoff plate theory, Reissner-Mindlin plate theory, and Reddy plate theory. The vibration of polar orthotropic circular plates on an elastic foundation has been investigated by Gupta *et al*. (1994). The Mindlin shear deformable plate theory was employed and the Chebyshev collocation method was applied to obtain the frequency parameters for the circular plates. Ju and Lee (1995) developed a finite element model to study the vibration of Mindlin plates with multiple stepped variations in thickness and resting on non-homogeneous elastic foundations. Gupta *et al*. (Gupta *et al*. 1990, Gupta and Ansari 2002) studied the effect of elastic foundation on axisymmetric vibrations of polar orthotropic circular plates of variable thickness by taking approximating polynomials in Rayleigh–Ritz method. Laura and Gutierrez (1991) analyzed the free vibration of a solid circular plate of linearly varying thickness attached to Winkler foundation using the Ritz method. Matsunaga (2008) analyzed the natural frequencies and buckling stresses of FG plates using a higher order shear deformation theory which are based on the through the thickness series expansion of the displacement components. Zhou *et al*. (2004) used Ritz method to analyze the free-vibration characteristics of rectangular thick plates resting on elastic foundations. Matsunaga (2000) investigated a two-dimensional, higher-order theory for analyzing the thick simply

supported rectangular plates resting on elastic foundations. Liew *et al*. (1996) employed the differential quadrature method for studying the Mindlin's plate on Winkler foundation. Cheng and Batra (2000) used Reddy's third-order plate theory to study steady state vibrations and buckling of a simply supported functionally gradient isotropic polygonal plate resting on a Pasternak elastic foundation and subjected to uniform in-plane hydrostatic loads. Malekzadeh (2009) studied free vibration analyses of functionally graded plates on elastic foundations based on the three-dimensional elasticity.

In structural mechanics, one of the most popular semi-analytical methods is differential quadrature method (DQM), remarkable success of which has been demonstrated in many research works including vibration analysis of plates (Tahouneh 2014a, b, Tahouneh and Naei 2014, Tahouneh and Yas 2012, 2013, 2014, Tahouneh *et al*. 2013, Yas and Tahouneh 2012), shells (Tahouneh and Naei 2015a), and even sandwich structures (Tahouneh and Naei 2015b). The differential quadrature method (DQM) is found to be a simple and efficient numerical technique for structural analysis. Better convergence behavior is observed by DQM compared with its peer numerical competent techniques viz. the finite element method, the finite difference method, the boundary element method and the meshless technique.

This paper is motivated by the lack of studies in the technical literature concerning to the three-dimensional vibration analysis of a continuously graded carbon nanotube-reinforced (CGCNTR) rectangular plates resting on a two-parameter foundation. To the authors' best knowledge, research on the vibration of thick a continuously graded carbon nanotube-reinforced (CGCNTR) rectangular plates resting on a two-parameter foundation based on the three-dimensional theory of elasticity has not been seen until now. In this study, the volume fractions of oriented, straight single-walled carbon nanotubes (SWCNTs) are assumed to be graded in the thickness direction. An equivalent continuum model based on the Eshelby-Mori-Tanaka approach is employed to estimate the effective constitutive law of the elastic isotropic medium (matrix) with dispersed elastic inhomogeneities (oriented CNTs). A sensitivity analysis is performed, and the natural frequencies are calculated for different sets of boundary conditions and different combinations of the geometric, and foundation parameters. Therefore, very complex combinations of the material properties, boundary conditions, and foundation stiffness are considered in the present semi-analytical solution approach.

2. Problem description

Consider a CGCNTR rectangular plate with length a, width b, and thickness h as depicted in Fig. 1. The plate is supported by an elastic foundation with Winkler's (normal) and Pasternak's (shear) coefficients. The deformations defined with reference to a Cartesian coordinate system (x, y, z) are u, v and w in the x, y and z directions, respectively. We assume that CGCNTR rectangular plate is made from a mixture of oriented, straight SWCNT, graded distribution in the thickness direction, and polymer matrix which is assumed to be isotropic (Shi *et al*. 2004).

2.1 Estimation of effective material properties of CNTRC

In this research work, we exploit an equivalent continuum model based on the Eshelby-Mori-Tanaka approach in order to estimate the effective constitutive law of the elastic isotropic medium (matrix) with dispersed elastic inhomogeneities (carbon nanotubes). The major step towards

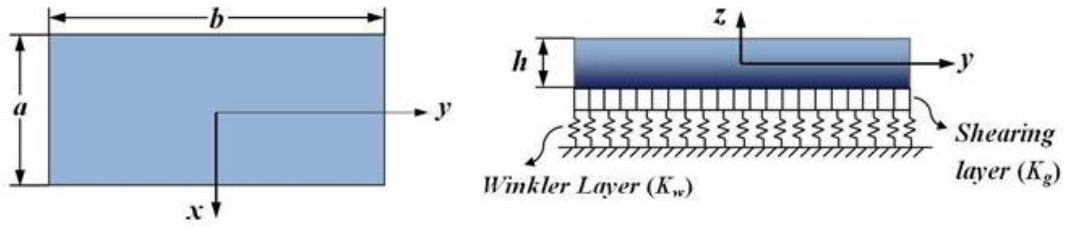

Fig. 1 The sketch of an elastically supported thick continuously graded carbon nanotube reinforced rectangular plate and setup of the coordinate system

modeling materials with fully dispersed inhomogeneities was undertaken by Mori and Tanaka (1973). In particular, they accounted for the presence of multiple inclusions and boundary conditions and their interactions. Giordano *et al*. (2009) used the homogenization procedure, based on the Eshelby theory, under small deformations and small volume fractions of the embedded phases, to determine the bulk and shear moduli and Landau coefficients of the composite material. Previous studies had established the validity of the Eshelby-Mori-Tanaka approach in determining the effective properties of composites reinforced with misaligned, carbon fibres, and with carbon nanotubes (Odegard *et al*. 2003, Benveniste 1987, Chen and Cheng 1996). In this paper, the proposed model is framed with the Eshelby theory for elastic inclusions. The original theory of Eshelby (1957, 1959) is restricted to one single inclusion in a semi-infinite elastic, homogeneous and isotropic medium. The theory, generalized by Mori-Tanaka, allows to extend the original approach to the practical case of multiple inhomogeneities embedded into a finite domain. The Eshelby-Mori-Tanaka approach, based on the equivalent elastic inclusion idea of Eshelby and the concept of average stress in the matrix due to Mori-Tanaka, is also known as the equivalent inclusion-average stress method (Formica *et al*. 2010).

2.1.1 Nanocomposite reinforced by aligned, straight CNTs

Consider a linear elastic polymer matrix reinforced by a large number of dispersed straight CNTs. First, we consider a polymer composite reinforced with aligned and straight CNTs. According to Benveniste's revisitation (1987), the following expression of the effective elastic tensor is obtained

$$C = C_m + f_r \langle (C_r - C_m) A_r \rangle \left(f_m I + f_r \langle A_r \rangle \right)^{-1} \tag{1}$$

where f_r and f_m are the fiber and matrix volume fractions, respectively, I is the identity tensor, C_m is the stiffness tensor of the matrix material, C_r is the stiffness tensor of the equivalent fiber, and A_r is the dilute mechanical strain concentration tensor for the fiber

$$A_r = \left[I + S(C_m)^{-1}(C_r - C_m) \right]^{-1} \tag{2}$$

the tensor S is Eshelby's tensor, as given by Eshelby (1957) and Mura (1982). The terms enclosed with angle brackets in Eq. (1) represent the average value of the term over all orientations defined by transformation from the local fiber coordinates ($o - x_1' x_2' x_3'$) to the global coordinates ($o - x_1 x_2 x_3$), Fig. 2. The matrix is assumed to be elastic and isotropic, with Young's modulus E_m and Poisson's ratio υ_m. Each straight CNT is modeled as a long fiber with transversely isotropic elastic properties.

Therefore, the composite is also transversely isotropic. The substitution of non-vanishing components of the Eshelby tensor S for a straight, long fiber along the x_2- direction in Eq. (2) gives the dilute mechanical strain concentration tensor. Then the substitution of A_r (Eq. (2)) into Eq. (1) gives the tensor of effective elastic moduli of the composite reinforced by aligned and straight CNTs. In particular, the Hill's elastic moduli are found as (Shi *et al*. 2004)

$$k = \frac{E_m\{E_m f_m + 2k_r(1+\upsilon_m)[1+f_r(1-2\upsilon_m)]\}}{2(1+\upsilon_m)[E_m(1+f_r-2\upsilon_m)+2f_m k_r(1-\upsilon_m-2\upsilon_m^2)]} \tag{3}$$

$$l = \frac{E_m\{\upsilon_m f_m[E_m + 2k_r(1+\upsilon_m)]+2f_r k_r(1-\upsilon_m^2)\}}{(1+\upsilon_m)[E_m(1+f_r-2\upsilon_m)+2f_m k_r(1-\upsilon_m-2\upsilon_m^2)]} \tag{4}$$

$$n = \frac{E_m^2 f_m(1+f_r-f_m\upsilon_m)+2f_m f_r(k_r n_r - l_r^2)(1+\upsilon_m)^2(1-2\upsilon_m)}{(1+\upsilon_m)[E_m(1+f_r-2\upsilon_m)+2f_m k_r(1-\upsilon_m-2\upsilon_m^2)]} + \frac{E_m[2f_m^2 k_r(1-\upsilon_m)+f_r n_r(1+f_r-2\upsilon_m)-4f_m l_r\upsilon_m]}{E_m(1+f_r-2\upsilon_m)+2f_m k_r(1-\upsilon_m-2\upsilon_m^2)} \tag{5}$$

$$p = \frac{E_m[E_m f_m + 2p_r(1+\upsilon_m)(1+f_r)]}{2(1+\upsilon_m)[E_m(1+f_r)+2f_m p_r(1+\upsilon_m)]} \tag{6}$$

$$k = \frac{E_m[E_m f_m + 2m_r(1+\upsilon_m)(3+f_r-4\upsilon_m)]}{2(1+\upsilon_m)\{E_m[f_m+4f_r(1-\upsilon_m)]+2f_m m_r(3-\upsilon_m-4\upsilon_m^2)\}} \tag{7}$$

where k, l, m, n, and p are Hill's elastic moduli of the composite; k is the plane-strain bulk modulus normal to the fiber direction, n is the uniaxial tension modulus in the fiber direction, l is the associated cross modulus, m and p are the shear moduli in planes normal and parallel to the fiber direction, respectively. k_r , l_r , m_r , n_r , and p_r are the Hill's elastic moduli for the reinforcing phase (CNTs). The elastic moduli parallel and normal to CNTs are related to Hill's elastic moduli by

$$E_{\square} = n - \frac{l^2}{k} \quad , E_{\perp} = \frac{4m(kn-l^2)}{kn-l^2+mn} \tag{8}$$

2.1.2 Nanocomposite reinforced by oriented, straight CNTs

In this section, the influence of oriented, straight CNTs is investigated. The orientation of a straight CNT is characterized by two Euler angles α and β, as shown in Fig. 2. The orientation distribution of CNTs in the CNTRC is characterized by a probability density function for oriented nanotubes in which case the composite is isotropic. The base vectors e_i and e_i' of the global ($o-x_1x_2x_3$) and the local coordinate systems ($o-x_1'x_2'x_3'$) are related via the transformation matrix g

$$e_i = g_{ij} e_j' \tag{9}$$

where g is given by

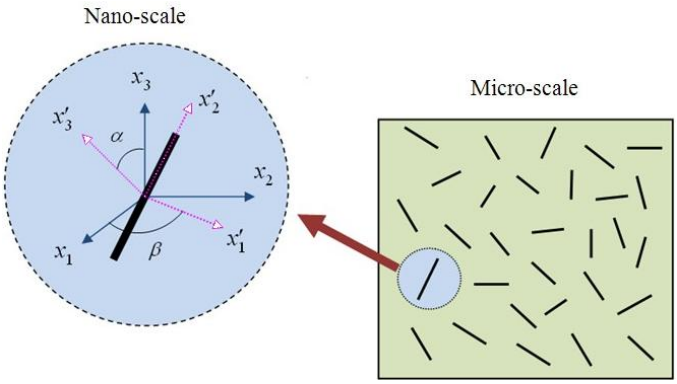

Fig. 2 Representative volume element (RVE) including straight CNTs

$$g = \begin{bmatrix} \cos\beta & -\cos\alpha\sin\beta & \sin\alpha\sin\beta \\ \sin\beta & \cos\alpha\cos\beta & -\sin\alpha\cos\beta \\ 0 & \sin\alpha & \cos\alpha \end{bmatrix} \tag{10}$$

The orientation distribution of CNTs in a composite is characterized by a probability density function $P(\alpha, \beta)$ satisfying the normalization condition (Shi *et al*. 2004)

$$\int_0^{2\pi}\int_0^{\pi/2} p(\alpha,\beta)\sin\alpha \;\; d\alpha \;\; d\beta = 1 \tag{11}$$

If CNTs are completely oriented, the density function is

$$p(\alpha,\beta) = \frac{1}{2\pi} \tag{12}$$

According to the Mori-Tanaka method, the strain $\varepsilon_r(\alpha, \beta)$ and the stress $\sigma_r(\alpha, \beta)$ of the CNT are related to the stress of matrix σ_m by

$$\begin{aligned} \varepsilon_r(\alpha,\beta) &= A(\alpha,\beta)\varepsilon_m = A(\alpha,\beta)C_m^{-1}\sigma_m, \\ \sigma_r(\alpha,\beta) &= C_r A(\alpha,\beta)\varepsilon_m = [C_r A(\alpha,\beta)C_m^{-1}]\sigma_m \end{aligned} \tag{13}$$

where the strain concentration tensor $A(\alpha, \beta)$ is given by Eq. (2). Then the average strain and stress in all oriented CNTs can be written as

$$\begin{aligned} \langle\varepsilon_r\rangle &= \left[\int_0^{2\pi}\int_0^{\pi/2} p(\alpha,\beta)A(\alpha,\beta)\sin\alpha \;\; d\alpha \;\; d\beta\right]\varepsilon_m, \\ \langle\sigma_r\rangle &= \left[\int_0^{2\pi}\int_0^{\pi/2} p(\alpha,\beta)\left[C_r A(\alpha,\beta)C_m^{-1}\right]\sin\alpha \;\; d\alpha \;\; d\beta\right]\sigma_m \end{aligned} \tag{14}$$

The angle brackets represent the average over special orientations. Using the average theorems $\sigma = f_m\sigma_m + f_r\langle\sigma_r\rangle$ and $\varepsilon = f_m\sigma_m + f_r\langle\sigma_r\rangle$ in conjunction with the effective constitutiverelation $\sigma = C\varepsilon$,

one can get the effective modulus of the composite according to Eq. (1).When CNTs are completely oriented in the matrix, the composite is then isotropic, and itsbulk modulus K and shear modulus G are derived as

$$K = K_m + \frac{V_f\,(\delta_r - 3K_m\alpha_r)}{3(V_m - V_f\,\alpha_r)} \tag{15}$$

$$G = G_m + \frac{V_f\,(\eta_r - 2G_m\beta_r)}{2(V_m - V_f\,\beta_r)} \tag{16}$$

where

$$\alpha_r = \frac{3(K_m + G_m) + k_r + l_r}{3(k_r + G_m)} \tag{17}$$

$$\beta_r = \frac{1}{5}\left[\frac{4G_m + 2k_r + l_r}{3(G_m + k_r)} + \frac{4G_m}{G_m + p_r} + \frac{2\left[G_m(3K_m + G_m) + G_m(3K_m + 7G_m)\right]}{G_m(3K_m + G_m) + m_r(3K_m + 7G_m)}\right] \tag{18}$$

$$\delta_r = \frac{1}{3}\left[n_r + 2l_r + \frac{(2k_r + l_r)(3K_m + 2G_m - l_r)}{G_m + k_r}\right] \tag{19}$$

$$\eta_r = \frac{1}{5}\left[\frac{2}{3}(n_r - l_r) + \frac{8G_m p_r}{G_m + p_r} + \frac{2(k_r - l_r)(2G_m + l_r)}{3(G_m + k_r)}\right] + \frac{1}{5}\left[\frac{8m_r G_m(3K_m + 4G_m)}{3K_m(m_r + G_m) + G_m(7m_r + G_m)}\right] \tag{20}$$

where K_m and G_m are the bulk and shear moduli of the matrix, respectively. k_r, m_r, n_r and l_r are the Hill's elastic moduli for the reinforcing phase. The effective Young's modulus E and Poisson's ratio υ of the material are given by

$$E = \frac{9KG}{3K + G} \tag{21}$$

$$\upsilon = \frac{3K - 2G}{6K + 2G} \tag{22}$$

In addition, V_f and V_m are the volume fractions of the CNTs and the matrix, which satisfy the relationship of $V_f + V_m = 1$. Similarly, mass density ρ can be calculated by

$$\rho = \rho_f V_f + \rho_m V_m \tag{23}$$

where ρf and ρm are the mass density of the CNTs and the matrix, respectively.

In order to examine the effect of different CNTs distribution on the free vibration characteristics of CGCNTR rectangular plates resting on elastic foundations, various types of material profiles through the plate thickness ($\eta_z = z/h$) are considered. In this work, we assume

only linear distribution of CNTs volume fraction for the different types of the CGCNTR rectangular plate, as follow

$$CGCNTR-\mathbb{V}:\ V_f = 2\left[\frac{z}{h}+0.5\right]V_f^* \tag{24}$$

$$CGCNTR-\Lambda:\ V_f = -2\left[\frac{z}{h}-0.5\right]V_f^* \tag{25}$$

$$CGCNTR-\mathbb{X}:\ V_f = 4\left[\frac{|z|}{h}\right]V_f^* \tag{26}$$

$$CGCNTR-\Diamond:\ V_f = 4\left[0.5-\frac{|z|}{h}\right]V_f^* \tag{27}$$

where V_f^* is the volume fraction of CNTs (Fidelus *et al*. 2005, Shen 2009, 2011) that is calculated from the mass fraction of nanotubes, m_f, assuming two phases and no trapped air, using (Fidelus *et al*. 2005)

$$V_f^* = \left[\frac{\rho_r}{m_f}-\rho_r+1\right]^{-1} \tag{28}$$

where $\rho_r = \rho_f/\rho_m$ is the ratio of nanotube to matrix density. Note that $V_f = V_f^*$ corresponds to the uniformly distributed CNTR rectangular plate, referred to as CNTR-UD. With V_f^* defined in Eq. (28), both the CGCNTR plate and CNTR-UD plate have the same value of CNTs mass fraction. For type *V*, the top surface of the plate ($\eta_z = 0.5$) is CNT-rich, referred to as CGCNTR-V (Fig. 3).

As can be seen from Fig. 3, for type Λ, the distribution of CNTs reinforcements is inversed and the bottom surface of the plate ($\eta_z = -0.5$) is CNT-rich, referred to as CGCNTR- Λ. For type X, a mid-plane symmetric graded distribution of CNTs reinforcements is achieved and both top and

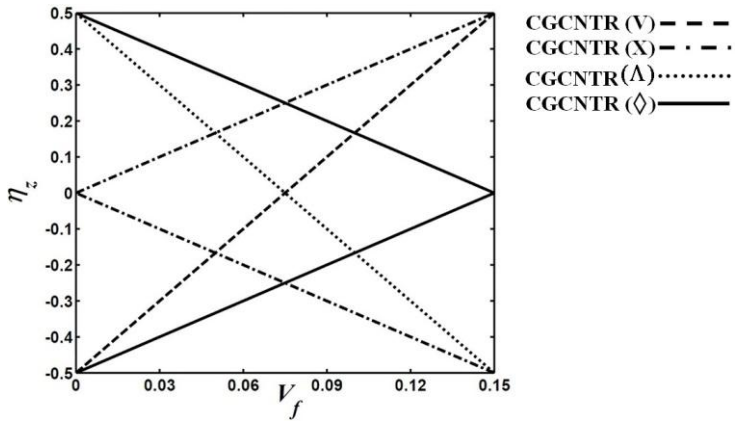

Fig. 3 Variations of CNTs volume fractions through the thickness of the plate for different types of CNT distribution

bottom surfaces are CNT-rich, referred to as CGCNTR-X. For type ◊, the distribution of CNTs reinforcements is inversed and both top and bottom surfaces are CNT-poor, whereas the reference surface ($\eta_z = 0$) is CNT-rich, referred to as CGCNTR-◊.

3. Theoretical formulations

The mechanical constitutive relations that relate the stresses to the strains are as follows (Fung and Tong 2001)

$$\sigma_{ij} = \lambda\varepsilon_{kk}\,\delta_{ij} + 2\mu\varepsilon_{ij} \tag{29}$$

where λ and μ are the Lame constants, ε_{ij} is the infinitesimal strain tensor and δ_{ij} is the Kronecker delta. In the absence of body forces, the equations of motion are as follows

$$\begin{aligned}
&\frac{\partial\sigma_x}{\partial x}+\frac{\partial\tau_{xy}}{\partial y}+\frac{\partial\tau_{xz}}{\partial z}=\rho\frac{\partial^2 u}{\partial t^2},\\
&\frac{\partial\tau_{xy}}{\partial x}+\frac{\partial\sigma_y}{\partial y}+\frac{\partial\tau_{yz}}{\partial z}=\rho\frac{\partial^2 v}{\partial t^2},\\
&\frac{\partial\tau_{xz}}{\partial x}+\frac{\partial\tau_{yz}}{\partial y}+\frac{\partial\sigma_z}{\partial z}=\rho\frac{\partial^2 w}{\partial t^2}
\end{aligned} \tag{30}$$

The infinitesimal strain tensor is related to the displacements as follows

$$\begin{aligned}
&\varepsilon_x=\frac{\partial u}{\partial x},\varepsilon_y=\frac{\partial v}{\partial y},\varepsilon_z=\frac{\partial w}{\partial z},\gamma_{xy}=\frac{\partial u}{\partial y}+\frac{\partial v}{\partial x},\\
&\gamma_{xz}=\frac{\partial u}{\partial z}+\frac{\partial w}{\partial x},\gamma_{yz}=\frac{\partial v}{\partial z}+\frac{\partial w}{\partial y}
\end{aligned} \tag{31}$$

where u, v and w are displacement components along the x, y and z axes, respectively. Upon substitution Eq. (31) into Eq. (29) and then into Eq. (30), the following equations of motion are obtained in terms of displacement components

$$\begin{aligned}
&c_{11}\frac{\partial^2 u}{\partial x^2}+c_{12}\frac{\partial^2 v}{\partial x\,\partial y}+c_{13}\frac{\partial^2 w}{\partial x\,\partial z}+c_{66}\left(\frac{\partial^2 v}{\partial y\,\partial x}+\frac{\partial^2 u}{\partial y^2}\right)+\\
&\frac{\partial c_{55}}{\partial z}\left(\frac{\partial w}{\partial x}+\frac{\partial u}{\partial z}\right)+c_{55}\left(\frac{\partial^2 w}{\partial z\,\partial x}+\frac{\partial^2 u}{\partial z^2}\right)=\rho\frac{\partial^2 u}{\partial t^2}
\end{aligned} \tag{32}$$

$$\begin{aligned}
&c_{66}\left(\frac{\partial^2 v}{\partial x^2}+\frac{\partial^2 u}{\partial x\,\partial y}\right)+c_{12}\frac{\partial^2 u}{\partial y\,\partial x}+c_{22}\frac{\partial^2 v}{\partial y^2}+c_{23}\frac{\partial^2 w}{\partial y\,\partial z}+\\
&\frac{\partial c_{44}}{\partial z}\left(\frac{\partial v}{\partial z}+\frac{\partial w}{\partial y}\right)+c_{44}\left(\frac{\partial^2 v}{\partial z^2}+\frac{\partial^2 w}{\partial z\,\partial y}\right)=\rho\frac{\partial^2 v}{\partial t^2}
\end{aligned} \tag{33}$$

$$c_{55}(\frac{\partial^2 w}{\partial x^2}+\frac{\partial^2 u}{\partial x\,\partial z})+c_{44}(\frac{\partial^2 v}{\partial y\,\partial z}+\frac{\partial^2 w}{\partial y^2})+\frac{\partial c_{13}}{\partial z}\frac{\partial u}{\partial x}+$$
$$c_{13}\frac{\partial^2 u}{\partial z\,\partial x}+\frac{\partial c_{23}}{\partial z}\frac{\partial v}{\partial y}+c_{23}\frac{\partial^2 v}{\partial z\,\partial y}+\frac{\partial c_{33}}{\partial z}\frac{\partial w}{\partial z}+c_{33}\frac{\partial^2 w}{\partial z^2}=\rho\frac{\partial^2 w}{\partial t^2} \tag{34}$$

Eqs. (32) and (33) represent the in-plane equations of motion along the *x*- and *y*- axes, respectively; and Eq. (34) is the transverse or out-of-plane equation of motion. The related boundary conditions at $z = -h/2$ and $h/2$ are as follows

at $z = -h/2$

$$\sigma_{zx}=0,$$
$$\sigma_{zy}=0,\sigma_{zz}=K_w w-K_g(\frac{\partial^2 w}{\partial x^2}+\frac{\partial^2 w}{\partial y^2}) \tag{35}$$

at $z = h/2$

$$\sigma_{zx}=0,$$
$$\sigma_{zy}=0, \tag{36}$$
$$\sigma_{zz}=0$$

where σ_{ij} are the components of stress tensor; K_w and K_g are Winkler and shearing layer elastic coefficients of the foundation. Different types of classical boundary conditions at the edges of the plate can be stated as

- Simply supported (*S*)

$$\sigma_{yy}=0,\quad w=0,\quad u=0; \tag{37}$$

- Clamped (*C*)

$$u=0,\quad v=0,\quad w=0; \tag{38}$$

- Free (*F*)

$$\sigma_{yy}=0,\quad \sigma_{xy}=0,\quad \sigma_{yz}=0 \tag{39}$$

Here, plates with two opposite edges at $x = -a/2$ and $a/2$ simply supported and arbitrary conditions at edges $y = -b/2$ and $b/2$ are considered. For free vibration analysis, by adopting the following form for the displacement components the boundary conditions at edges $x = -a/2$ and $a/2$ are satisfied.

$$u(x,y,z,t)=U_m(y,z,t)\cos(m\pi(x+a/2)/a)e^{i\omega t},$$
$$v(x,y,z,t)=V_m(y,z,t)\sin(m\pi(x+a/2)/a)e^{i\omega t}, \tag{40}$$
$$w(x,y,z,t)=W_m(y,z,t)\sin(m\pi(x+a/2)/a)e^{i\omega t}$$

where *m* is the wave number along the *x*-direction, ω is the natural frequency and i $(=\sqrt{-1})$ is the imaginary number. Substituting for displacement components from Eq. (40) into Eqs. (32)-(34), the coupled partial differential equations are reduced to a set of coupled ordinary differential

equations (ODE) as follows:

Eq. (32)

$$-c_{11}(\frac{m\pi}{a})^2U_m+c_{12}(\frac{m\pi}{a})\frac{\partial V_m}{\partial y}+c_{13}(\frac{m\pi}{a})\frac{\partial W_m}{\partial z}+c_{66}(\frac{m\pi}{a}\frac{\partial V_m}{\partial y}+\frac{\partial^2 U_m}{\partial y^2})+\frac{\partial c_{55}}{\partial z}(\frac{m\pi}{a}W_m+\frac{\partial U_m}{\partial z})+c_{55}(\frac{m\pi}{a}\frac{\partial W_m}{\partial z}+\frac{\partial^2 U_m}{\partial z^2})=-\rho\omega^2U_m \tag{41}$$

Eq. (33)

$$c_{66}(-(\frac{m\pi}{a})^2V_m-(\frac{m\pi}{a})\frac{\partial U_m}{\partial y})+c_{12}(\frac{-m\pi}{a})\frac{\partial U_m}{\partial y}+c_{22}\frac{\partial^2 V_m}{\partial y^2}+c_{23}\frac{\partial^2 W_m}{\partial y\partial z}+\frac{\partial c_{44}}{\partial z}(\frac{\partial V_m}{\partial z}+\frac{\partial W_m}{\partial y})+c_{44}(\frac{\partial^2 V_m}{\partial z^2}+\frac{\partial^2 W_m}{\partial z\partial y})=-\rho\omega^2V_m \tag{42}$$

Eq. (34)

$$c_{55}(-(\frac{m\pi}{a})^2W_m-(\frac{m\pi}{a})\frac{\partial U_m}{\partial z})+c_{44}(\frac{\partial^2 V_m}{\partial y\partial z}+\frac{\partial^2 W_m}{\partial y^2})+\frac{\partial c_{13}}{\partial z}(-\frac{m\pi}{a}U_m)+c_{13}(-\frac{m\pi}{a}\frac{\partial U_m}{\partial z})+\frac{\partial c_{23}}{\partial z}\frac{\partial V_m}{\partial y}+c_{23}\frac{\partial^2 V_m}{\partial z\partial y}+\frac{\partial c_{33}}{\partial z}\frac{\partial W_m}{\partial z}+c_{33}\frac{\partial^2 W_m}{\partial z^2}=-\rho\omega^2W_m \tag{43}$$

The geometrical and natural boundary conditions stated in Eqs. (35)-(39) can also be simplified, however, for brevity purpose they are not shown here.

4. DQM solution for equations of motion and boundary conditions

It is necessary to develop appropriate methods to investigate the mechanical responses of continuously graded carbon nanotube-reinforced structures. But, due to the complexity of the problem, it is difficult to obtain the exact solution. In this paper, the differential quadrature method (DQM) approach is used to solve the governing equations of continuously graded carbon nanotube-reinforced (CGCNTR) rectangular plates. One can compare DQM solution procedure with the other two widely used traditional methods for plate analysis, i.e., Rayleigh-Ritz method and FEM. The main difference between the DQM and the other methods is how the governing equations are discretized. In DQM the governing equations and boundary conditions are directly discretized, and thus elements of stiffness and mass matrices are evaluated directly. But in Rayleigh-Ritz and FEMs, the weak form of the governing equations should be developed and the boundary conditions are satisfied in the weak form. Generally by doing so larger number of integrals with increasing amount of differentiation should be done to arrive at the element matrices. Also, the number of degrees of freedom will be increased for an acceptable accuracy. The basic idea of the DQM is the derivative of a function, with respect to a space variable at a given sampling point, is approximated as a weighted linear sum of the sampling points in the domain of that variable. In order to illustrate the DQ approximation, consider a function $f(\xi, \eta)$ defined on a rectangular domain $0 \le \xi \le a$ and $0 \le \eta \le b$. Let in the given domain, the function values be known or desired on a grid of sampling points. According to DQM method, the rth derivative of the function $f(\xi, \eta)$ can be approximated as

$$\frac{\partial^r f(\xi,\eta)}{\partial \xi^r}\Big|_{(\xi,\eta)=(\xi_i,\eta_j)} = \sum_{m=1}^{N_\xi} A_{im}^{\xi(r)} f(\xi_m,\eta_j) = \sum_{m=1}^{N_\xi} A_{im}^{\xi(r)} f_{mj} \tag{44}$$

For $i = 1, 2, \ldots, N_\xi$ and $r = 1, 2, \ldots, N_\xi - 1$

where N_ξ represents the total number of nodes along the ξ-direction. From this Equation one can deduce that the important components of DQM approximations are the weighting coefficients $(A_{ij}^{\xi(r)})$ and the choice of sampling points. In order to determine the weighting coefficients a set of test functions should be used in Eq. (44). The weighting coefficients for the first-order derivatives in ξ-direction are thus determined as (Bert and Malik 1996)

$$A_{ij}^{\xi} = \begin{cases} \dfrac{1}{a}\dfrac{M(\xi_i)}{(\xi_i-\xi_j)M(\xi_j)} & for \quad i \neq j \\ -\sum\limits_{\substack{j=1 \\ i\neq j}}^{N_\xi} A_{ij}^{\xi} & for \quad i = j \end{cases} ; i, j = 1,2,\ldots, N_\xi \tag{45}$$

where

$$M(\xi_i) = \prod_{j=1, i\neq j}^{N_\xi} (\xi_i - \xi_j) \tag{46}$$

The weighting coefficients of the second-order derivative can be obtained in the matrix form (Bert and Malik 1996)

$$\left[B_{ij}^{\xi}\right] = \left[A_{ij}^{\xi}\right]\left[A_{ij}^{\xi}\right] = \left[A_{ij}^{\xi}\right]^2 \tag{47}$$

In a similar manner, the weighting coefficients for the η-direction can be obtained.

The natural and simplest choice of the grid points is equally spaced points in the direction of the coordinate axes of computational domain. It was demonstrated that non-uniform grid points gives a better result with the same number of equally spaced grid points (Bert and Malik 1996). It is shown (Shu and Wang 1999) that one of the best options for obtaining grid points is Chebyshev–Gauss–Lobatto quadrature points

$$\frac{\xi_i}{a} = \frac{1}{2}\left\{1 - \cos\left[\frac{(i-1)\pi}{(N_\xi - 1)}\right]\right\}, \frac{\eta_j}{b} = \frac{1}{2}\left\{1 - \cos\left[\frac{(j-1)\pi}{(N_\eta - 1)}\right]\right\} \tag{48}$$

For $i = 1, 2, \ldots, N_\xi$; $j = 1, 2, \ldots, N_\eta$

where N_ξ and N_η are the total number of nodes along the ξ- and η-directions, respectively.

At this stage, the DQ method can be applied to discretize the equations of motion (41-43) and the boundary conditions. As a result, at each domain grid point (y_i, z_k) with $j = 2,\ldots, N_y - 1$ and $k = 2,\ldots, N_z - 1$, the discretized equations take the following forms

Eq. (41)

$$
\begin{aligned}
&-(c_{11})_{jk}\left(\frac{m\pi}{a}\right)^2 U_{mjk}+(c_{12})_{jk}\left(\frac{m\pi}{a}\right)\sum_{n=1}^{N_y}A_{jn}^{y}V_{mnk}+(c_{13})_{jk}\left(\frac{m\pi}{a}\right)\\
&\sum_{n=1}^{N_z}A_{kn}^{z}W_{mjn}+(c_{66})_{jk}\left(\frac{m\pi}{a}\sum_{n=1}^{N_y}A_{jn}^{y}V_{mnk}+\sum_{n=1}^{N_y}B_{jn}^{y}U_{mnk}\right)+\left(\frac{\partial c_{55}}{\partial z}\right)_{jk}\\
&\left(\frac{m\pi}{a}W_{mjk}+\sum_{n=1}^{N_z}A_{kn}^{z}U_{mjn}\right)+(c_{55})_{jk}\left(\frac{m\pi}{a}\sum_{n=1}^{N_z}A_{kn}^{z}W_{mjn}+\sum_{n=1}^{N_z}B_{kn}^{z}U_{mjn}\right)\\
&=-\rho_{jk}\,\omega^2 U_{mjk}
\end{aligned}
\tag{49}
$$

Eq. (42)

$$
\begin{aligned}
&(c_{66})_{jk}\left(-\left(\frac{m\pi}{a}\right)^2 V_{mjk}+\left(\frac{-m\pi}{a}\right)\sum_{n=1}^{N_y}A_{jn}^{y}U_{mnk}\right)+(c_{12})_{jk}\left(\left(\frac{-m\pi}{a}\right)\right.\\
&\left.\sum_{n=1}^{N_y}A_{jn}^{y}U_{mnk}\right)+(c_{22})_{jk}\sum_{n=1}^{N_y}B_{jn}^{y}V_{mnk}+(c_{23})_{jk}\left(\sum_{n=1}^{N_y}\sum_{r=1}^{N_z}A_{kr}^{z}A_{jn}^{y}W_{mnr}\right)+\\
&\left(\frac{\partial c_{44}}{\partial z}\right)_{jk}\left(\sum_{n=1}^{N_z}A_{kn}^{z}V_{mjn}+\sum_{n=1}^{N_y}A_{jn}^{y}W_{mnk}\right)+(c_{44})_{jk}\left(\sum_{n=1}^{N_z}B_{kn}^{z}V_{mjn}+\right.\\
&\left.\sum_{n=1}^{N_y}\sum_{r=1}^{N_z}A_{kr}^{z}A_{jn}^{y}W_{mnr}\right)=-\rho_{jk}\,\omega^2 V_{mjk}
\end{aligned}
\tag{50}
$$

Eq. (43)

$$
\begin{aligned}
&(c_{55})_{jk}\left(-\left(\frac{m\pi}{a}\right)^2 W_{mjk}-\frac{m\pi}{a}\sum_{n=1}^{N_z}A_{kn}^{z}U_{mjn}\right)+(c_{44})_{jk}\\
&\left(\sum_{n=1}^{N_y}\sum_{r=1}^{N_z}A_{kr}^{z}A_{jn}^{y}V_{mnr}+\sum_{n=1}^{N_y}B_{jn}^{y}W_{mnk}\right)+\left(\frac{\partial c_{13}}{\partial z}\right)_{jk}\left(-\frac{m\pi}{a}\right.\\
&\left.U_{mjk}\right)+(c_{13})_{jk}\left(-\frac{m\pi}{a}\sum_{n=1}^{N_z}A_{kn}^{z}U_{mjn}\right)+\left(\frac{\partial c_{23}}{\partial z}\right)_{jk}\sum_{n=1}^{N_y}A_{jn}^{y}V_{mnk}\\
&+(c_{23})_{jk}\sum_{n=1}^{N_y}\sum_{r=1}^{N_z}A_{kr}^{z}A_{jn}^{y}V_{mnr}+\left(\frac{\partial c_{33}}{\partial z}\right)_{jk}\sum_{n=1}^{N_z}A_{kn}^{z}W_{mjn}+(c_{33})_{jk}\\
&\sum_{n=1}^{N_z}B_{kn}^{z}W_{mjn}=-\rho_{jk}\,\omega^2 W_{mjk}
\end{aligned}
\tag{51}
$$

where A_{ij}^{y}, A_{ij}^{z} and B_{ij}^{y}, B_{ij}^{z} are the first and second order DQ weighting coefficients in the *y*- and *z*-directions, respectively. In a similar manner the boundary conditions can be discretized. For

this purpose, using Eq. (40) and the DQ discretization rules for spatial derivatives, the boundary conditions at $z = -h/2$ and $h/2$ become,

at $z = -h/2$

$$\begin{gathered}(\frac{m\pi}{a})W_{mjk} + \sum_{n=1}^{N_z} A_{kn}^z U_{mjn} = 0, \sum_{n=1}^{N_y} A_{jn}^y W_{mnk} + \sum_{n=1}^{N_z} A_{kn}^z V_{mjn} = 0, \\ (c_{13})_{jk}(\frac{-m\pi}{a})U_{mjk} + (c_{23})_{jk}\sum_{n=1}^{N_y} A_{jn}^y V_{mnk} + (c_{33})_{jk}\sum_{n=1}^{N_z} A_{kn}^z W_{mjn} \\ -k_w W_{mjk} + k_g(-W_{mjk}(\frac{m\pi}{a})^2 + \sum_{n=1}^{N_y} B_{jn}^y W_{mnk}) = 0\end{gathered} \tag{52}$$

at $z = h/2$

$$\begin{gathered}(\frac{m\pi}{a})W_{mjk} + \sum_{n=1}^{N_z} A_{kn}^z U_{mjn} = 0, \sum_{n=1}^{N_y} A_{jn}^y W_{mnk} + \sum_{n=1}^{N_z} A_{kn}^z V_{mjn} = 0, \\ (c_{13})_{jk}(\frac{-m\pi}{a})U_{mjk} + (c_{23})_{jk}\sum_{n=1}^{N_y} A_{jn}^y V_{mnk} + (c_{33})_{jk}\sum_{n=1}^{N_z} A_{kn}^z W_{mjn} = 0\end{gathered} \tag{53}$$

where $k = 1$ at $z = -h/2$ and $k = N_z$ at $z = h/2$, and $j = 1,2,\ldots, N_y$.

The boundary conditions at $y = -b/2$ and $b/2$ become,

- Simply supported (*S*)

$$\begin{gathered}U_{mjk} = 0, W_{mjk} = 0, \\ -(c_{12})_{jk}(\frac{m\pi}{a})U_{mjk} + (c_{22})_{jk}\sum_{n=1}^{N_y} A_{jn}^y V_{mnk} + (c_{23})_{jk}\sum_{n=1}^{N_z} A_{kn}^z W_{mjn} = 0\end{gathered} \tag{54}$$

- Clamped (C)

$$U_{mjk} = 0, V_{mjk} = 0, W_{mjk} = 0 \tag{55}$$

- Free (F)

$$\begin{gathered}(c_{12})_{jk}(\frac{-m\pi}{a})U_{mjk} + (c_{22})_{jk}\sum_{n=1}^{N_y} A_{jn}^y V_{mnk} + (c_{23})_{jk}\sum_{n=1}^{N_z} A_{kn}^z W_{mjn} = 0, \\ (\frac{m\pi}{a})V_{mjk} + \sum_{n=1}^{N_y} A_{jn}^y U_{mnk} = 0, \sum_{n=1}^{N_z} A_{kn}^z V_{mjn} + \sum_{n=1}^{N_y} A_{jn}^y W_{mnk} = 0\end{gathered} \tag{56}$$

In the above equations $k = 2,\ldots, N_z-1$; also $j = 1$ at $y = -b/2$ and $j = N_y$ at $y = b/2$.

In order to carry out the eigenvalue analysis, the domain and boundary nodal displacements should be separated. In vector forms, they are denoted as $\{d\}$ and $\{b\}$, respectively. Based on this definition, the discretized form of the equations of motion and the related boundary conditions can

be represented in the matrix form as:

Eqs. of motion (49)-(51)

$$[[K_{db}][K_{dd}]]\begin{Bmatrix}\{b\}\\ \{d\}\end{Bmatrix}-\omega^2[M]\{d\}=\{0\} \tag{57}$$

Boundary conditions (52)-(53) and (54)-(56)

$$[K_{bd}]\{d\}+[K_{bb}]\{b\}=\{0\} \tag{58}$$

Eliminating the boundary degrees of freedom in Eq. (57) using Eq. (58), this Equation becomes

$$[K]-\omega^2[M]\{d\}=\{0\} \tag{59}$$

where $[K] = [K_{dd}] – [K_{db}][K_{bb}]^{-1}[K_{bd}]$. The above eigenvalue system of equations can be solved to find the natural frequencies and mode shapes of the plate.

5. Numerical results and discussion

5.1 Convergence and comparison studies

Due to lack of appropriate results for free vibration of continuously graded carbon nanotube-reinforced (CGCNTR) rectangular plates resting on a two-parameter foundation for direct comparison, validation of the presented formulation is conducted in two ways. Firstly, the results are compared with those of 1-D conventional functionally graded rectangular plates, and then, the results of the presented formulations are given in the form of convergence studies with respect to N_z and N_y, the number of discrete points distributed along the thickness and width of the plate, respectively. The boundary conditions of the plate are specified by the letter symbols, for example, *S-C-S-F* denotes a plate with edges $x = –a/2$ and $a/2$ simply supported (*S*), edge $y = –b/2$ clamped (*C*) and edge $y = b/2$ free (*F*).

As a first example, the properties of the plate are assumed to vary through the thickness of the plate with a desired variation of the volume fractions of the two materials in between the two surfaces. The modulus of elasticity E and mass density ρ are assumed to be in terms of a simple power law distribution and Poisson's ratio υ is assumed to be constant as follows

$$\begin{aligned} &E(z)=E_M+E_{CM}V_f,\ \ \upsilon(z)=\upsilon_0\ \ \ \rho(z)=\rho_M+\rho_{CM}V_f,\\ &E_{CM}=E_C-E_M,\ \ \rho_{CM}=\rho_C-\rho_M,\ \ V_f=(0.5+z/h)^p \end{aligned} \tag{60}$$

where $–h/2 \le z \le h/2$ and p is the power law index which takes values greater than or equal to zero. Subscripts M and C refer to the metal and ceramic constituents which denote the material properties of the bottom and top surface of the plate, respectively. The mechanical properties are as follows:

- Metal (Aluminum, Al)

$$E_M=70*10^9\ N/m^2,\upsilon=0.3,\rho_M=2702\,kg/m^3.$$

Table 1 Convergence behavior and accuracy of the first seven non-dimensional natural frequencies ($\varpi = \omega h\sqrt{\rho_C / E_C}$) of a simply supported FG plate against the number of DQ grid points (b/h = 2)

P	N_z	N_y	ϖ_1	ϖ_2	ϖ_3	ϖ_4	ϖ_5	ϖ_6	ϖ_7
0	7	7	0.5569	0.9395	0.9735	1.3764	1.5072	1.6064	1.7384
		9	0.5570	0.9396	0.9741	1.3771	1.5083	1.6071	1.7401
		13	0.5570	0.9396	0.9740	1.3774	1.5088	1.6076	1.7407
	9	7	0.5573	0.9398	0.9735	1.3771	1.5087	1.6074	1.7403
		9	0.5572	0.9400	0.9742	1.3777	1.5090	1.6079	1.7406
		13	0.5572	0.9400	0.9741	1.3778	1.5096	1.6086	1.7405
	13	7	0.5571	0.9401	0.9735	1.3779	1.5094	1.6083	1.7411
		9	0.5572	0.9400	0.9742	1.3777	1.5090	1.6078	1.7405
		13	0.5572	0.9400	0.9742	1.3777	1.5090	1.6078	1.7406
		(Matsunaga 2008)	0.5572	0.9400	0.9742	1.3777	1.5090	1.6078	1.7406
0.5	7	7	0.4829	0.8222	0.8700	1.2250	1.3332	1.4364	1.5401
		9	0.4828	0.8229	0.8707	1.2258	1.3337	1.4367	1.5429
		13	0.4830	0.8224	0.8706	1.2254	1.3338	1.4370	1.5424
	9	7	0.4833	0.8225	0.8701	1.2251	1.3335	1.4365	1.5402
		9	0.4835	0.8240	0.8708	1.2257	1.3340	1.4370	1.5431
		13	0.4836	0.8233	0.8707	1.2258	1.3340	1.4369	1.5426
	13	7	0.4836	0.8227	0.8701	1.2251	1.3334	1.4366	1.5402
		9	0.4835	0.8231	0.8708	1.2259	1.3338	1.4370	1.5431
		13	0.4835	0.8233	0.8709	1.2259	1.3339	1.4370	1.5425
		(Matsunaga 2008)	0.4835	0.8233	0.8709	1.2259	1.3339	1.4370	1.5425
1	7	7	0.4367	0.7476	0.7997	1.1158	1.2154	1.3085	1.4059
		9	0.4374	0.7477	0.8001	1.1165	1.2159	1.3090	1.4075
		13	0.4373	0.7478	0.8005	1.1163	1.2162	1.3088	1.4077
	9	7	0.4368	0.7477	0.7998	1.1159	1.2157	1.3088	1.4068
		9	0.4374	0.7477	0.8003	1.1165	1.2161	1.3090	1.4076
		13	0.4374	0.7478	0.8006	1.1165	1.2162	1.3090	1.4078
	13	7	0.4368	0.7477	0.7999	1.1159	1.2158	1.3088	1.4070
		9	0.4375	0.7478	0.8003	1.1165	1.2162	1.3091	1.4076
		13	0.4375	0.7478	0.8005	1.1165	1.2163	1.3091	1.4077
		(Matsunaga 2008)	0.4375	0.7477	0.8005	1.1166	1.2163	1.3091	1.4078
4	7	7	0.3565	0.5988	0.6249	0.8724	0.9589	1.0000	1.1029
		9	0.3577	0.5995	0.6355	0.8729	0.9589	1.0007	1.1038
		13	0.3577	0.5996	0.6349	0.8728	0.9589	1.0003	1.1030
	9	7	0.3569	0.5989	0.6250	0.8726	0.9589	1.0001	1.1032
		9	0.3579	0.5997	0.6357	0.8731	0.9589	1.0008	1.1040
		13	0.3578	0.5997	0.6351	0.8730	0.9589	1.0005	1.1032

Table 1 Continued

P	N_z	N_y	ϖ_1	ϖ_2	ϖ_3	ϖ_4	ϖ_5	ϖ_6	ϖ_7
4	13	7	0.3571	0.5991	0.6252	0.8727	0.9589	1.0001	1.1033
		9	0.3579	0.5997	0.6357	0.8731	0.9589	1.0008	1.1040
		13	0.3579	0.5997	0.6352	0.8731	0.9589	1.0008	1.1040
		(Matsunaga 2008)	0.3579	0.5997	0.6352	0.8731	0.9591	1.0008	1.1040
10	7	7	0.3306	0.5454	0.5657	0.7866	0.8588	0.9043	0.9838
		9	0.3311	0.5460	0.5662	0.7890	0.8588	0.9047	0.9841
		13	0.3310	0.5459	0.5661	0.7881	0.8588	0.9050	0.9846
	9	7	0.3308	0.5455	0.5659	0.7870	0.8588	0.9044	0.9840
		9	0.3313	0.5461	0.5664	0.7892	0.8588	0.9048	0.9842
		13	0.3312	0.5460	0.5663	0.7883	0.8588	0.9051	0.9846
	13	7	0.3309	0.5455	0.5660	0.7871	0.8588	0.9045	0.9840
		9	0.3313	0.5461	0.5664	0.7892	0.8588	0.9049	0.9844
		13	0.3313	0.5461	0.5664	0.7884	0.8588	0.9051	0.9847
		(Matsunaga 2008)	0.3313	0.5460	0.5664	0.7885	0.8588	0.9050	0.9847

- Ceramic (Alumina, Al_2O_3)

$$E_C = 380*10^9\ N/m^2, \upsilon = 0.3, \rho_C = 3800\,kg/m^3.$$

In Table 1, the first seven non-dimensional natural frequency parameters of simply supported thick FG plate are compared with those of Matsunaga (2008)

As the second example, in order to validate the results for plates on an elastic foundation, the results for the first three natural frequency parameters of isotropic thick plate with two different values of thickness-to-length ratios and different values of Winkler elastic coefficient are presented in Table 2. They are compared with those of Zhou *et al*. (2004), Matsunaga (2000). In this example the non-dimensional natural frequency, Winkler and shearing layer elastic coefficients are as follows

$$\begin{gathered}\lambda = \omega\frac{b^2}{\pi^2}\sqrt{\rho_C h/D_C}, D_C = E_C h^3/12(1-\upsilon_C^2),\\ k_g = K_g b^2/D_C, k_w = K_w b^4/D_C\end{gathered} \tag{61}$$

According to the data presented in the above-mentioned tables, excellent solution agreements can be observed between the present method and those of the other methods. Based on the above studies, a numerical value of $N_z = N_y = 13$ is used for the next studies.

In this study, the non-dimensional natural frequency, Winkler and shearing layer elastic coefficients are as follows

$$\begin{gathered}\Omega = \omega\frac{b^2}{\pi^2}\sqrt{\rho_m h/D_m}, D_m = E_m h^3/12(1-\upsilon_m^2),\\ k_g = K_g b^2/D_m, k_w = K_w b^4/D_m\end{gathered} \tag{62}$$

Table 2 Comparison of the first three non-dimensional natural frequency parameters of a simply supported square isotropic plate on the elastic foundation (kg = 10)

K_w	N_z	N_y	b/h = 2			b/h = 5		
			λ_{11}	λ_{12}	λ_{13}	λ_{11}	λ_{12}	λ_{13}
0	7	7	1.6453	2.6906	3.8259	2.2325	4.4045	7.2429
		9	1.6461	2.6855	3.8264	2.2332	4.4058	7.2434
		13	1.6460	2.6848	3.8264	2.2330	4.4052	7.2433
	9	7	1.6455	2.6905	3.8261	2.2329	4.4046	7.2431
		9	1.6462	2.6857	3.8267	2.2334	4.4060	7.2436
		13	1.6461	2.6850	3.8266	2.2333	4.4055	7.2435
	13	7	1.6455	2.6907	3.8262	2.2330	4.4049	7.2432
		9	1.6462	2.6857	3.8267	2.2334	4.4060	7.2436
		13	1.6462	2.6851	3.8267	2.2334	4.4057	7.2436
		(Zhou *et al*. 2004)	1.6462	2.6851	3.8268	2.2334	4.4056	7.2436
		(Matsunaga 2000)	1.6462	2.6851	3.8268	2.2334	4.4056	7.2436
10	7	7	1.6569	2.6870	3.8261	2.2532	4.415	7.2474
		9	1.6575	2.6875	3.8280	2.2537	4.415	7.2484
		13	1.6574	2.6875	3.8271	2.2536	4.415	7.2483
	9	7	1.6572	2.6872	3.8262	2.2534	4.415	7.2481
		9	1.6577	2.6878	3.8282	2.2539	4.415	7.2487
		13	1.6576	2.6876	3.8273	2.2538	4.415	7.2485
	13	7	1.6573	2.6873	3.8264	2.2535	4.415	7.2482
		9	1.6577	2.6878	3.8282	2.2539	4.415	7.2487
		13	1.6577	2.6878	3.8275	2.2539	4.415	7.2487
		(Zhou *et al*. 2004)	1.6577	2.6879	3.8274	2.2539	4.415	7.2487
		(Matsunaga 2000)	1.6577	2.6879	3.8274	2.2539	4.415	7.2488

where ρ_m, E_m and υ_m are mechanical properties of matrix. In this work, Poly (methyl methacrylate), referred to as PMMA, is selected for the matrix, and the material properties of which are assumed to be, υ_m = 0.34 and E_m = 2.5 GPa (Shen 2011, Wang and Shen 2011). The (10,10) SWCNTs are selected as reinforcements. The material properties of the (10, 10) SWCNTs used here from Refs. (Shen and Zhang, Shen 2011, Wang and Shen 2011), E_f^{11} = 5.6466 Tpa, E_f^{22} = 7.08 Tpa, G_f^{12} = 1.9445 Tpa and υ_f^{12} = 0.175 at room temperature (300 K).

5.2 Parametric studies

After demonstrating the convergence and accuracy of the method, parametric studies for 3-D vibration analysis of elastically supported thick CGCNTR rectangular plates reinforced by oriented CNTs for different CNTs distributions and various length to width ratio (a/b) and different combinations of free, simply supported and clamped boundary conditions at the edges, are computed. Fig. 4 shows the effect of the CNTs volume fraction V_f^* on CGCNTR-V to CNTR-UD

fundamental frequency ratio, $\Omega_{11}^{CG}/\Omega_{11}^{UD}$, of the nanocomposite rectangular plates for different values of b/h ratios. Three different values of the CNTs volume fraction V_f^* = 0.12, 0.17 and 0.28 are taken into account. Correspondingly, the CNTs mass fractions are m_f = 0.142, 0.2 and 0.321, respectively, by taking the density of CNT ρ_f = 1.4 g/cm^3 and the density of matrix ρ_m = 1.15 g/cm^3 in Eq. (28). It can be seen that the discrepancies between the frequencies for the plates with continuously graded and uniform distribution of CNTs increases with the increase of the CNTs volume fraction V_f^*. This figure is also shown that the discrepancies between the frequencies decrease with the increase of the b/h ratio. It should be noted that this behavior is also observed at other boundary conditions, but, for the sale of brevity, we consider only two types of the boundary conditions.

The variation of $\Omega_{11}^{CG}/\Omega_{11}^{UD}$ ratio of the S-C-S-C nanocomposite rectangular plates with b/h and a/b ratios is shown in Fig. 5. As it is observed, the $\Omega_{11}^{CG}/\Omega_{11}^{UD}$ ratio decreases rapidly with the

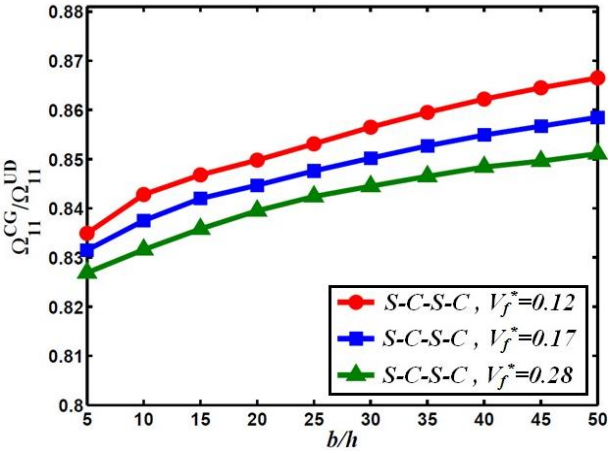

Fig. 4 Variation of the $\Omega_{11}^{CG}/\Omega_{11}^{UD}$ ratios of the nanocomposite plate for different values of b/h ratios and different values of the CNTs volume fraction (a/b = 5, K_g = 10, K_w = 100)

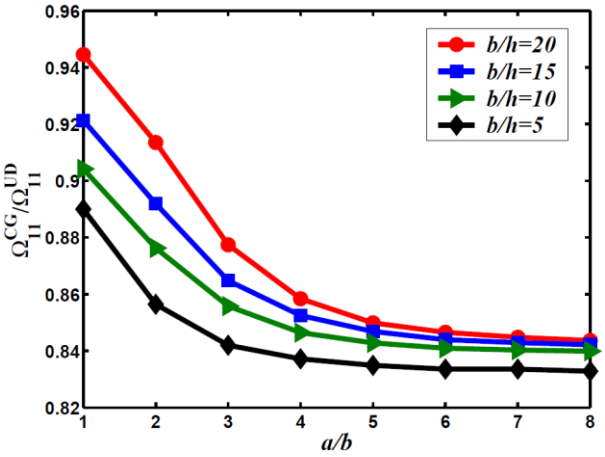

Fig. 5 Variations of the $\Omega_{11}^{CG}/\Omega_{11}^{UD}$ ratios of the S-C-S-C nanocomposite rectangular plate for different values of a/b and b/h ratios (V_f^* = 0.12, K_g = 10, K_w = 100)

increase of a/b ratio and then remains almost unaltered for $a/b > 7$. It is observed that when the b/h ratios become smaller, the discrepancies between the frequencies for CGCNTR-V and CNTR-UD rectangular plates become larger.

In Fig. 6, the effect of various boundary conditions on the $\Omega_{11}^{CG}/\Omega_{11}^{UD}$ ratios of the nanocomposite rectangular plates with $V_f^* = 0.12$ for different values of a/b ratios is depicted. It can also be inferred from Fig. 6 that the S-C-S-C CGCNTR rectangular plate has the highest, whereas the S-F-S-F one has the lowest $\Omega_{11}^{CG}/\Omega_{11}^{UD}$ ratio values, implying that the discrepancies between the frequencies of CGCNTR and CNTR-UD rectangular plate with greater supporting rigidity will be lower. In addition, Fig. 6 reveals that effects of the boundary conditions on the $\Omega_{11}^{CG}/\Omega_{11}^{UD}$ ratio diminish as a/b ratio increases.

In Figs. 7 and 8 the effects of variation of wave number (m) on the frequency parameters of S-C-S-C CGCNTR-V rectangular plate with $V_f^* = 0.12$ for different values of a/b and b/h ratios are

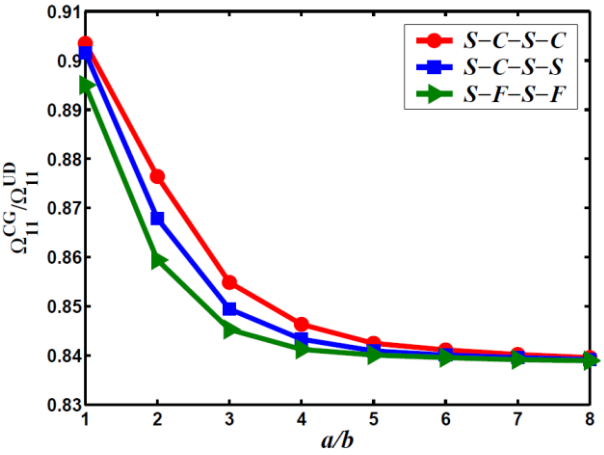

Fig. 6 Effect of various boundary conditions on the $\Omega_{11}^{CG}/\Omega_{11}^{UD}$ ratios of the nanocomposite rectangular plate for different values of a/b ratios ($V_f^* = 0.12$, $K_g = 10$, $K_w = 100$, $b/h = 10$)

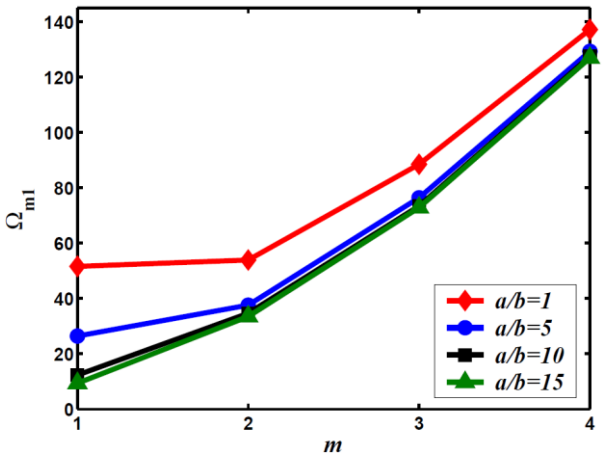

Fig. 7 Variation of wave number (m) with the frequency parameters of S-C-S-C CGCNTR-V nanocomposite rectangular plate for different values of a/b ratios ($V_f^* = 0.12$, $K_g = 10$, $K_w = 100$, $b/h = 10$)

demonstrated. According to Fig. 7, the general behavior of the frequency parameters of CGCNTR rectangular plate for all *a*/*b* ratios is that the frequency parameters converge only in the range beyond that of the fundamental frequency parameters. This means that the effects of *a*/*b* ratios are more prominent at low wave numbers, particularly those in the range before that of the fundamental frequency parameters, that at high wave numbers. As in Fig. 8 is shown, when the wave number increases the discrepancies between the frequency parameters for the different values of *b*/*h* ratios become larger. It should be noted at this point that this natural frequency behavior contrasts with the natural frequency behavior of the CGCNTR rectangular plate for different values of *a*/*b* ratios. This behavior is also observed at other boundary conditions that again are not shown here for brevity. In the following discussion, the effect of different types of CNTs distributions through the plate thickness on the free vibration characteristics of CGCNTR rectangular plate is investigated.

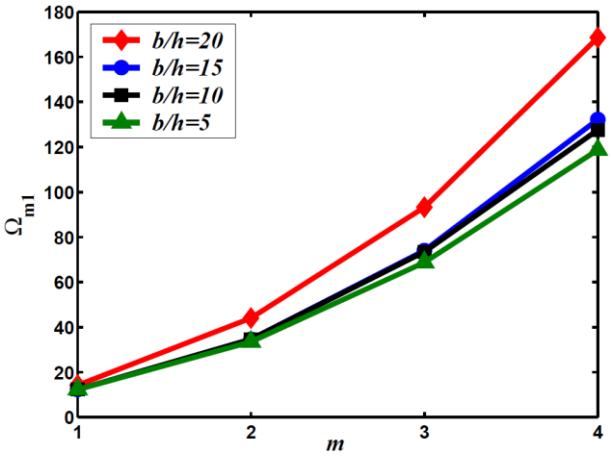

Fig. 8 Variation of wave number (*m*) with the frequency parameters of S-C-S-C CGCNTR-V nanocomposite rectangular plate for different values of *b*/*h* ratio (V_f^* = 0.12, K_g = 10, K_w = 100, *b*/*h* = 10)

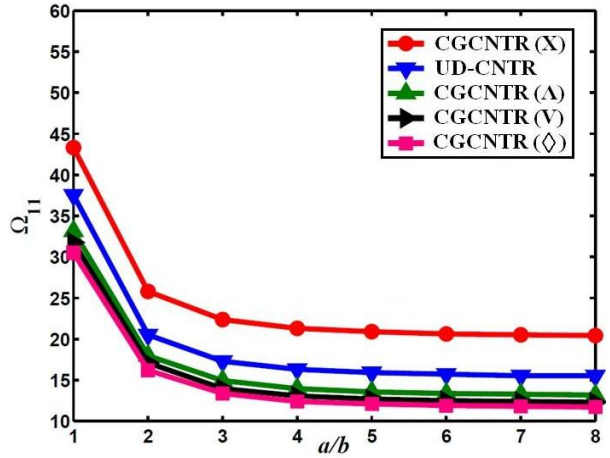

Fig. 9 Variation of the frequency parameters versus *a*/*b* ratios with different types of CNTs distribution for S-C-S-C nanocomposite rectangular plate (V_f^* = 0.12, K_g = 10, K_w = 100, *b*/*h* = 10)

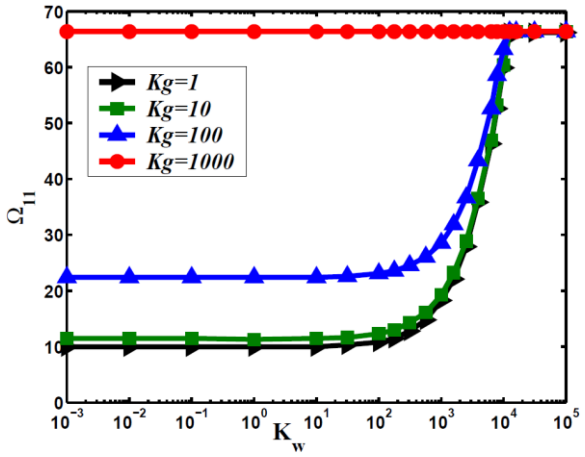

Fig. 10 Variations of fundamental frequency parameters of a S-C-S-C nanocomposite rectangular plate resting on a two-parameter elastic foundation with Winkler and different shearing layer elastic coefficient (V_f^* = 0.12, a/b = 10, b/h = 10)

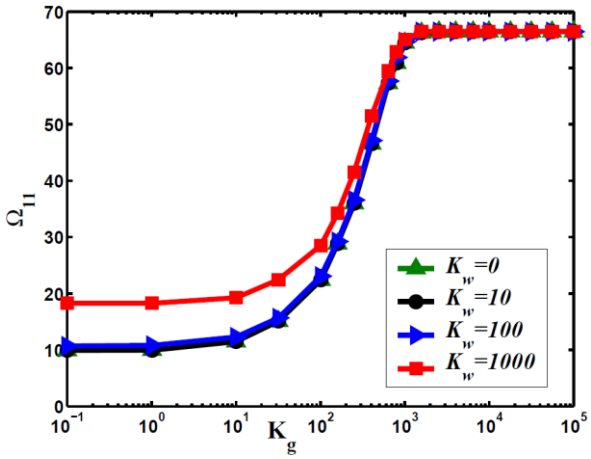

Fig. 11 Variations of fundamental frequency parameters of a S-C-S-C nanocomposite rectangular plate versus the shearing layer elastic coefficient for different Winkler elastic coefficient (V_f^* = 0.12, a/b = 10, b/h = 10)

In Fig. 9, the influence of a/b ratios on the fundamental frequency parameters of the S-C-S-C nanocomposite rectangular plate with V_f^* = 0.12 for different types of CNTs distributions is depicted. As can be seen from this figure, the lowest frequency parameters is obtained by using CGCNTR-◊ volume fractions profile. On the contrary, oriented, straight CNTs with CGCNTR-X profile has the maximum value of the frequency parameter.

Fig. 10 shows the effects of variation of the Winkler elastic coefficient on the fundamental frequency parameters of the S-C-S-C nanocomposite rectangular plate and for different values of shearing layer elastic coefficient. It is clear that with increasing the elastic coefficients of the foundation, the frequency parameters increase to some limit values. It is observed for the large values of Winkler elastic coefficient, the shearing layer elastic coefficient has less effect and the

results become independent of it.

The influence of shearing layer elastic coefficient on the fundamental frequency parameters is shown in Fig. 11. One can see that the Winkler elastic coefficient has little effect on the fundamental frequency parameters at different values of shearing layer elastic coefficient. This behavior is also observed at other boundary conditions, but, for the sale of brevity, we consider only this type of the boundary condition.

6. Conclusions

In this research work, differential quadrature method was employed to obtain a highly accurate semi-analytical solution for free vibration of nanocomposite rectangular plates resting on a two-parameter elastic foundation under various boundary conditions. The study was carried out based on the three-dimensional, linear and small strain elasticity theory. The volume fractions of oriented, straight single-walled carbon nanotubes (SWCNTs) were assumed to be graded in the thickness direction. The Eshelby-Mori-Tanaka approach was used to estimate the effective constitutive law of the elastic isotropic medium (matrix) with oriented, straight CNTs. The impacts of the volume fractions of oriented CNTs, different CNTs distributions, geometrical parameters and elastic coefficients of foundation on the vibrational characteristics of elastically supported thick rectangular plates were investigated. From this study, some conclusions can be made:

- Based on the achieved results, the continuously graded CNTs volume fractions can be utilized for the management of vibrational behavior of structures so that the frequency parameters of structures made of such material can be considerably improved than the nanocomposites reinforced with uniformly distributed CNTs.
- The discrepancies between the frequencies for the plates with continuously graded and uniformly distributed CNTs decrease with the increase of the b/h ratio, but increase with increase in the CNTs volume fraction V_f^*.
- The discrepancies between the natural frequencies of the continuously graded and uniformly distributed CNTs rectangular plate with greater supporting rigidity will be lower.
- It is shown that the uniform distribution of CNTs volume fractions has the higher frequencies than that of asymmetric distributions, CGCNTR-Λ and CGCNTR-V.
- The interesting results show that the graded CNTs volume fractions with symmetric distributions through the plate thickness have high capabilities to reduce/increase the natural frequency than uniformly and asymmetric distributions.
- It is shown that with increasing the elastic coefficients of the foundation, the fundamental frequency parameters to some limit values. It is observed for the large values of Winkler elastic coefficient, the shearing layer elastic coefficient has less effect and the results become independent of it.
- It is shown that the variation of Winkler elastic coefficient has little effect on the fundamental frequency parameters at different values of shearing layer elastic coefficient. It is clear that in all cases, with increasing the shearing layer elastic coefficient of the foundation, the frequency parameters increase to some limit values. It is observed for the large values of shearing layer elastic coefficient; the results become independent of it.

References

Aragh, B.S. and Yas, M.H. (2010a), “Static and free vibration analyses of continuously graded fiber-

reinforced cylindrical shells using generalized power-law distribution", *Acta Mech*., **215**(1-4), 155-173.
Aragh, B.S. and Yas, M.H. (2010b), "Three-dimensional analysis of thermal stresses in four-parameter continuous grading fiber reinforced cylindrical panels", *Int. J. Mech. Sci*., **52**(8), 1047-1063.
Batra, R.C. and Jin, J. (2005), "Natural frequencies of a functionally graded anisotropic rectangular plate", *J. Sound Vib*., **282**(1), 509-516.
Benveniste, Y. (1987), "A new approach to the application of Mori-Tanaka's theory in composite materials", *Mech. Mater*., **6**(2), 147-157.
Bert, C.W. and Malik, M. (1996), "Differential quadrature method in computational mechanics: A review", A review; *Appl. Mech. Rev*., **49**(1), 1-28.
Bonnet, P., Sireude, D., Garnier, B. and Chauvet, O. (2007), "Thermal properties and percolation in carbon nanotube-polymer composites", *J. Appl. Phys*., **91**(20), 1910.
Chang, T. and Gao, H. (2003), "Size-dependent elastic properties of a single-walled carbon nanotube via a molecular mechanics model", *J. Mech. Phys. Solids*, **51**(6), 1059-1074.
Chen, C.H. and Cheng, C.H. (1996), "Effective elastic moduli of misoriented short-fiber composites", *Int. J. Solids Struct*., **33**(17), 2519-2539.
Cheng, Z.Q. and Batra, R. (2000), "Exact correspondence between eigenvalues of membranes and functionally graded simply supported polygonal plates", *J. Sound Vib*., **229**(4), 879-895.
Endo, M., Hayashi, T., Kim, Y.A., Terrones, M. and Dresselhaus, M.S. (2004), "Applications of carbon nanotubes in the twenty–first century", *Trans. R. Soc. Lond A*, Mathematical, Physical and Engineering Sciences, **362**(1823), 2223-2238.
Esawi, A.M. and Farag, M.M. (2007), "Carbon nanotube reinforced composites: Potential and current challenges", *Mater. Des*., **28**(9), 2394-2401.
Eshelby, J.D. (1957), "The determination of the elastic field of an ellipsoidal inclusion, and related problems", *Proc. R. Soc. A, Mathematical, Physical and Engineering Sciences*, **241**(1226), 376-396. DOI: 10.1098/rspa.1957.0133
Eshelby, J.D. (1959), "The elastic field outside an ellipsoidal inclusion", *Proc. R. Soc. A*, Mathematical, Physical and Engineering Sciences, **252**(1271), 561-569. DOI: 10.1098/rspa.1959.0173
Fidelus, J.D., Wiesel, E., Gojny, F.H., Schulte, K. and Wagner, H.D. (2005), "Thermo-mechanical properties of randomly oriented carbon/epoxy nanocomposites", *Composites Part A*, **36**(11), 1555-1561.
Formica, G., Lacarbonara, W. and Alessi, R. (2010), "Vibrations of carbon nanotube-reinforced composites", *J. Sound Vib*., **329**(10), 1875-1889.
Fung, Y.c. and Tong, P. (2001), *Classical and Computational Solid Mechanics*, World Scientific.
Giordano, S., Palla, P.L. and Colombo, L. (2009), "Nonlinear elasticity of composite materials", *Eur. Phys. J. B*., **68**(1), 89-101.
Griebel, M. and Hamaekers, J. (2004), "Molecular dynamics simulations of the elastic moduli of polymer–carbon nanotube composites", *Mech. Eng*., **193**(17), 1773-1788.
Gupta, U. and Ansari, A. (2002), "Effect of elastic foundation on asymmetric vibration of polar orthotropic linearly tapered circular plates", *J. Sound Vib*., **254**(3), 411-426.
Gupta, U.S., Lal, R. and Jain, S.K. (1990), "Effect of elastic foundation on axisymmetric vibrations of polar orthotropic circular plates of variable thickness", *J. Sound Vib*., **139**(3), 503-513.
Gupta, U.S., Lal, R. and Sagar, R. (1994), "Effect of an elastic foundation on axisymmetric vibrations of polar orthotropic Mindlin circular plates", *Indian J. Pure Appl. Math*., **25**(12), 1317-1317.
Han, Y. and Elliott, J. (2007), "Molecular dynamics simulations of the elastic properties of polymer/carbon nanotube composites", *Comput. Mater. Sci*., **39**(2), 315-323.
Hu, N., Fukunaga, H., Lu, C., Kameyama, M. and Yan, B. (2005), "Prediction of elastic properties of carbon nanotube reinforced composites", *Proc. R. Soc. A, Mathematical, Physical and Engineering Sciences*, **461**(2058), 1685-1910.
Jabbari, M., Bahtui, A. and Eslami, M.R. (2006), "Axisymmetric mechanical and thermal stresses in thick long FGM cylinders", *J. Therm. Stresses*, **29**(7), 643-663.
Jin, Y. and Yuan, F. (2003), "Simulation of elastic properties of single-walled carbon nanotubes", *Compos. Sci. Technol*., **63**(11), 1507-1515.

Ju, F. and Lee, H.P.K.H. (1995), "Free vibration of plates with stepped variations in thickness on non-homogeneous elastic foundations", *J. Sound Vib.*, **183**(3), 533-545.
Ke, L.L., Yang, J. and Kitipornchai, S. (2010), "Nonlinear free vibration of functionally graded carbon nanotube-reinforced composite beams", *Compos. Struct.*, **92**(3), 676-683.
Laura, P.A. and Gutierrez, R.H. (1991), "Free vibrations of a solid circular plate of linearly varying thickness and attached to a Winkler foundation", *J. Sound Vib.*, **144**(1), 149-161.
Liew, K.M., Han, J.B., Xiao, Z.M. and Du, H. (1996), "Differential quadrature method for Mindlin plates on Winkler foundations", *Int. J. Mech. Sci.*, **38**(4), 405-421.
Malekzadeh, P. (2009), "Three-dimensional free vibration analysis of thick functionally graded plates on elastic foundations", *J. Compos. Struct.*, **89**(3), 367-373.
Matsunaga, H. (2000), "Vibration and stability of thick plates on elastic foundations", *J. Eng. Mech. ASCE*, **126**(1), 27-34.
Matsunaga, H. (2008), "Free vibration and stability of functionally graded plates according to a 2-D higher-order deformation theory", *Compos. Struct.*, **82**(4), 499-512.
Moniruzzaman, M. and Winey, K.I. (2006), "Polymer nanocomposites containing carbon nanotubes", *Macromolecules*, **39**(16), 5194-5205.
Mori, T. and Tanaka, K. (1973), "Average stress in matrix and average elastic energy of materials with misfitting inclusions", *Acta Metall.*, **21**(5), 571-574.
Mura, T. (1982), *Micromechanics of Defects in Solids*, Springer Science & Business Media.
Odegard, G.M., Gates, T.S, Wise, K.E., Park, C. and Siochi, E.J. (2003), "Constitutive modeling of nanotube–reinforced polymer composites", *Compos. Sci. Technol.*, **63**(11), 1671-1687.
Qian, D., Dickey, E.C., Andrews, R. and Rantell, T. (2000), "Load transfer and deformation mechanisms in carbon nanotube-polystyrene composites", *Appl. Phys. Lett.*, **76**(20), 2868-2870.
Reddy, J. and Cheng, Z.Q. (2001), "Three-dimensional thermomechanical deformations of functionally graded rectangular plates", *Eur. J. Mech. A/Solids*, **20**(5), 841-855.
Salvetat, D. and Rubio, A. (2002), "Mechanical properties of carbon nanotubes: A fiber digest for beginners", *Carbon*, **40**(10), 1729-1734.
Shen, H.S. (2009), "Nonlinear bending of functionally graded carbon nanotube-reinforced composite plates in thermal environments", *Compos. Struct.*, **91**(1), 9-19.
Shen, H.S. (2011), "Postbuckling of nanotube-reinforced composite cylindrical shells in thermal environments, Part I: Axially-loaded shells", *Compos. Struct.*, **93**(8), 2096-2108.
Shen, H.S. (2012), "Thermal buckling and postbuckling behavior of functionally graded carbon nanotube-reinforced composite cylindrical shells", C*ompos. Part B, Engineering*, **43**(3), 1030-1038.
Shen, H.S. and Zhang, C.L. (2010), "Thermal buckling and postbuckling behavior of functionally graded carbon nanotube-reinforced composite plates", *Mater. Des.*, **31**(7), 3403-3411.
Shen, H.S. and Zhu, Z.H. (2010), "Buckling and postbuckling behavior of functionally graded nanotube-reinforced composite plates in thermal environments", *Comput. Mater. Continua.*, **18**(2), 155-182.
Shi, D.L., Feng, X.Q., Huang, Y.Y., Hwang, K.C. and Gao, H. (2004), "The effect of nanotube waviness and agglomeration on the elastic property of carbon nanotube-reinforced composites", *J. Eng. Mater. Technol.*, **126**(3), 250-257.
Shu, C. and Wang, C. (1999), "Treatment of mixed and nonuniform boundary conditions in GDQ vibration analysis of rectangular plates", *Eng. Struct.*, **21**(2), 125-134.
Sobhani Aragh, B., Hedayati, H., Borzabadi Farahani, E. and Hedayati, M. (2011), "A novel 2-D six-parameter power-law distribution for free vibration and vibrational displacements of two-dimensional functionally graded fiber-reinforced curved panels", *Eur. J. Mech. A/Solids*, **30**(6), 865-883.
Tahouneh, V. (2014a), "Free vibration analysis of thick CGFR annular sector plates resting on elastic foundations", *Struct. Eng. Mech., Int. J.*, **50**(6), 773-796.
Tahouneh, V. (2014b), "Free vibration analysis of bidirectional functionally graded annular plates resting on elastic foundations using differential quadrature method", *Struct. Eng. Mech., Int. J.*, **52**(4), 663-686.
Tahouneh, V. and Naei, M.H. (2014), "A novel 2-D six-parameter power-law distribution for three-dimensional dynamic analysis of thick multi-directional functionally graded rectangular plates resting on

a two-parameter elastic foundation", *Meccanica*, **49**(1), 91-109.
Tahouneh, V. and Naei, M.H. (2015a), "3D free vibration analysis of elastically supported thick nanocomposite curved panels with finite length and different boundary conditions via 2-D GDQ method", *Mech. Adv. Mater. Struct.*, 1-80. DOI: 10.1080/15376494.2015.1068402
Tahouneh, V. and Naei, M.H. (2015b), "Free vibration and vibrational displacements analysis of thick elastically supported laminated curved panels with power-law distribution functionally graded layers and finite length via 2D GDQ method", *J. Sandw. Struct. Mater.*, 1-31. DOI: 10.1177/1099636215600709
Tahouneh, V. and Yas, M.H. (2012), "3-D free vibration analysis of thick functionally graded annular sector plates on Pasternak elastic foundation via 2-D differential quadrature method", *Acta Mech.*, **223**(9), 1879-1897.
Tahouneh, V. and Yas, M.H. (2013), "Semianalytical solution for three-dimensional vibration analysis of thick multidirectional functionally graded annular sector plates under various boundary conditions", *J. Eng. Mech.*, **140**(1), 31-46.
Tahouneh, V. and Yas, M.H. (2014), "Influence of equivalent continuum model based on the Eshelby-Mori-Tanaka scheme on the vibrational response of elastically supported thick continuously graded carbon nanotube-reinforced annular plates", *Polym. Composite*, **35**(8), 1644-1661.
Tahouneh, V., Yas, M.H., Tourang, H. and Kabirian, M. (2013), "Semi-analytical solution for three-dimensional vibration of thick continuous grading fiber reinforced (CGFR) annular plates on Pasternak elastic foundations with arbitrary boundary conditions on their circular edges", *Meccanica*, **48**(6), 1313-1336.
Thostenson, E.T., Ren, Z.F. and Chou, T.W. (2001), "Advances in the science and technology of carbon nanotubes and their composites", A Review; *Compos. Sci. Technol.*, **61**(13), 1899-1912.
Valter, B., Ram, M.K. and Nicolini, C. (2002), "Synthesis of multiwalled carbon nanotubes and poly (o-anisidine) nanocomposite material: Fabrication and characterization of its Langmuir-Schaefer films", *Langmuir*, **18**(5), 1535-1541.
Vel, S.S. (2010), "Exact elasticity solution for the vibration of functionally graded anisotropic cylindrical shells", *Compos. Struct.*, **92**(11), 2712-2727.
Vel, S.S. and Batra, R. (2004), "Three-dimensional exact solution for the vibration of functionally graded rectangular plates", *J. Sound. Vib.*, **272**(3), 703-730.
Wang, Z.X. and Shen, H.S. (2011), "Nonlinear vibration of nanotube-reinforced composite plates in thermal environments", *Comp. Mater. Sci.*, **50**(8), 2319-2330.
Wang, C.M., Kitipornchai, S. and Xiang, Y. (1997), "Relationships between buckling loads of Kirchhoff, Mindlin, and Reddy polygonal plates on Pasternak foundation", *J. Eng. Mech. ASCE*, **123**(11), 1134-1137.
Wernik, J. and Meguid, S. (2011), "Multiscale modeling of the nonlinear response of nano-reinforced polymers", *Acta Mech.*, **217**(1-2), 1-16.
Xiang, Y., Wang, C.M. and Kitipornchai, S. (1994), "Exact vibration solution for initially stressed Mindlin plates on Pasternak foundations", *Int. J. Mech. Sci.*, **36**(4), 311-316.
Xiang, Y., Kitipornchai, S. and Liew, K.M. (1996), "Buckling and vibration of thick laminates on Pasternak foundations", *J. Eng. Mech. ASCE*, **122**(1), 54-63.
Yas, M.H. and Sobhani Aragh, B. (2010), "Three-dimensional analysis for thermoelastic response of functionally graded fiber reinforced cylindrical panel", *Compos. Struct.*, **92**(10), 2391-2399.
Yas, M.H. and Tahouneh, V. (2012), "3-D free vibration analysis of thick functionally graded annular plates on Pasternak elastic foundation via differential quadrature method (DQM)", *Acta Mech.*, **223**(1), 43-62.
Yokozeki, T., Iwahori, Y. and Ishiwata, S. (2007), "Matrix cracking behaviors in carbon fiber/epoxy laminates filled with cup-stacked carbon nanotubes (CSCNTs)", *Composites Part A: Applied Science and Manufacturing*, **38**(3), 917-924.
Zhou, D., Cheung, Y.K., Lo, S.H. and Au, F.T.K. (2004), "Three-dimensional vibration analysis of rectangular thick plates on Pasternak foundation", *Int. J. Numer. Method. Eng.*, **59**(10), 1313-1334.

CC